

# Adiabatic Nanofocusing Scattering-Type Optical Nanoscopy of Individual Gold Nanoparticles

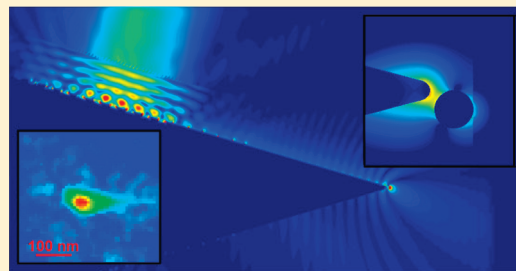
Diyar Sadiq,<sup>†</sup> Javid Shirdel,<sup>†</sup> Jae Sung Lee,<sup>‡</sup> Elena Selishcheva,<sup>†</sup> Namkyoo Park,<sup>‡</sup> and Christoph Lienau<sup>\*,†</sup>

<sup>†</sup>Institut für Physik, Carl von Ossietzky Universität, 26111 Oldenburg, Germany

<sup>‡</sup>Photonic Systems Laboratory, School of EECS, Seoul National University, Seoul 151-744, Korea

**ABSTRACT:** We explore imaging of local electromagnetic fields in the vicinity of metallic nanoparticles using a grating-coupled scattering-type near-field scanning optical microscope. In this microscope, propagating surface plasmon polariton wavepackets are launched onto smooth gold tapers where they are adiabatically focused toward the nanometer-sized taper apex. We report two-dimensional raster-scanned optical images showing pronounced near-field contrast and demonstrating sub-30 nm resolution imaging of localized surface plasmon polariton fields of spherical and elliptical nanoparticles. By comparison to three-dimensional finite-difference time domain simulations, we conclude that virtually background-free near-field imaging is achieved. The microscope combines deep subwavelength resolution, high local field intensities and a straightforward imaging contrast, making it interesting for a variety of applications in linear and nonlinear nanospectroscopy.

**KEYWORDS:** Surface plasmon polaritons, adiabatic nanofocusing, scattering-type near-field scanning optical microscopy, FDTD simulation, metallic nanoparticles



Scattering-type near-field scanning optical microscopy (s-NSOM)<sup>1–4</sup> is a powerful technique to overcome the classical diffraction limit in optical microscopy. It is now routinely used for (sub-) 10-nm-resolution imaging of surfaces in various wavelength regions from the visible,<sup>5–7</sup> and infrared,<sup>8–10</sup> to the terahertz<sup>11,12</sup> regime. In contrast to other approaches to near-field microscopy,<sup>13–15</sup> s-NSOM makes use of evanescent field confinement at the apex of a sharp metallic tip acting as a near-field probe. Typically, this field is created by focusing far field light directly onto the tip apex.

As a consequence of this direct tip illumination, the performance of present-day s-NSOM microscopes is often limited by a rather substantial signal background due to the scattering of the incident light from tip and/or sample. This background is routinely suppressed by tapping the tip against the sample and demodulating the collected light signal at the tapping frequency or its harmonics using different homodyne and heterodyne detection schemes.<sup>16–18</sup> Those techniques, however, are experimentally challenging and necessarily result in a loss of signal-to-noise ratio. Also, the interpretation of the image contrast is often rather involved.

A possible way to overcome these problems is to use a spatially nonlocal optical excitation of the tip apex by means of evanescent surface plasmon polariton (SPP) waves propagating along the taper shaft. Such an approach is based on the intriguing ability of adiabatic tapered plasmonic waveguides to focus optical energy into nanometer-sized spots at the taper apex.<sup>19,20</sup> Theoretically, SPP nanofocusing has been predicted and analyzed for metallic cones<sup>19–23</sup> and sharp metallic wedges.<sup>24–26</sup> On the experimental side, the effect has been studied in two-dimensional tapered waveguides<sup>27,28</sup> and also three-dimensional (3D) plasmonic nanofocusing has been demonstrated<sup>29,30</sup> by using grating-coupling to

launch SPPs onto a conical, gold taper several micrometers away from the tip apex. Such adiabatically focused light spots have already been used for tip-enhanced Raman spectroscopy,<sup>31,32</sup> partly with sub-10 nm resolution.<sup>31</sup> In an imaging application of such a SPP nanoemitter,<sup>33</sup> line scans across a silicon step edge demonstrated 20 nm resolution.

In this Letter, we report on using such a grating-coupled, adiabatically focused s-NSOM microscope for the first time for two-dimensional, modulation-free imaging of single metallic nanoparticles. We demonstrate sub-30 nm resolution imaging of localized SPP fields. By comparison to detailed theoretical simulations, we find that the image contrast in this microscope, governed solely by the interference between tip-scattered field and induced nanoparticle field, is particularly straightforward to interpret. Contributions from background stray fields are virtually absent.

Conceptually, we make use of a grating-coupler for launching SPPs onto an adiabatic gold taper.<sup>29</sup> The nanofocused SPP field confined to the tip apex locally probes the optical properties of the sample as shown schematically in Figure 1(a).

Slit gratings with 780 nm period, a slit width of 150 nm and a depth of 70–100 nm are focused-ion-beam milled onto the shaft of an electrochemically etched gold tip at a distance of 15  $\mu\text{m}$  from the tip apex. The grating on the tip shaft is illuminated with light from either a spectrally tunable continuous-wave or a mode-locked Ti:sapphire laser centered at 780 nm. The laser is linearly polarized in the direction perpendicular to the grooves in order

**Received:** December 30, 2010

**Revised:** February 23, 2011

**Published:** March 22, 2011

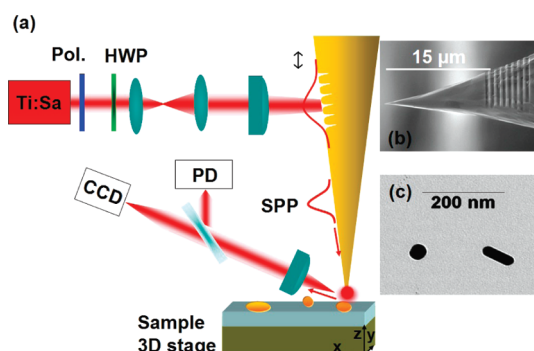


**Figure 1.** (a) Schematic of the adiabatic nanofocusing scattering-type optical microscope (s-NSOM). Light from a tunable Ti:sapphire laser at 780 nm passes through a polarizer (Pol.) and a half wave plate (HWP) and is focused by a high-NA objective onto a nanoslit grating milled onto the shaft of a gold taper. Light scattered from the tip apex into the far field is collected by a second high-NA objective in reflection geometry and imaged onto a photodetector. (b) Scanning electron micrograph of a conical gold tip with a 780 nm grating period prepared by focused ion beam milling. (c) Transmission electron microscopy image of a spherical and an elliptical gold nanoparticle.

to maximize the SPP excitation efficiency. The light is focused onto the tip shaft to a spot size of about  $6\ \mu\text{m}$  at close to normal incidence by a microscope objective with a numerical aperture (NA) of 0.35 and a working distance of 20 mm. As well-known, the grating transfers momentum  $k_g = 2\pi/a$ ,  $a$  is the grating period, to the incident light, thus allowing it to overcome the momentum mismatch between the incident light and SPPs. The excited SPP wave packets travel adiabatically along the taper surface toward the tip apex. Here, ideally, the wavepacket comes to a complete halt since both the phase and group velocity tend to zero for a tip with an arbitrarily small radius<sup>20</sup> and the field is localized and strongly enhanced at the apex. In reality, a finite radiation damping exists<sup>34</sup> and the SPP field localized at tip apex is scattered into the far field. In our setup, the scattered light from the tip is collected by a second microscope objective (NA = 0.5) and imaged onto a photodetector and a CDD camera. In the experiments, this scattered light is recorded while raster-scanning the nonlocally excited tip across the sample surface. For regulation of the distance between tip–sample, a shear-force-based feedback scheme is used in which the gold tip is mounted along the side of one of the arms of a quartz tuning fork. A hardware-linearized 3D piezo stage moves the sample with nanometric precision (Figure 1a).

In Figure 1b, a scanning electron microscope image of such a nanofabricated metal tip is shown. It is based on an electrochemically etched gold tip with a radius of curvature of less than 20 nm at the tip apex and an opening angle of  $30^\circ$ , slightly decreasing toward the tip apex. The optimum choice of the distance between the gratings and the tip apex (15–25  $\mu\text{m}$ ) is a trade-off between the propagation losses (the  $1/e$  decay length of SPPs for Au surface at 780 nm is about  $40\ \mu\text{m}$ )<sup>35</sup> and the reduction in the background signal due to the scattering from the shaft. This distance allows us to easily separate the excitation spot over the gratings and the scattered light from the tip apex using far-field optics. In the chosen geometry, grating scattering to the detection optics is negligible. We have experimented with different opening angles and the one chosen here was found to give good near-field contrast, reducing light scattering from the shaft and optimizing field localization at the tip apex. At normal

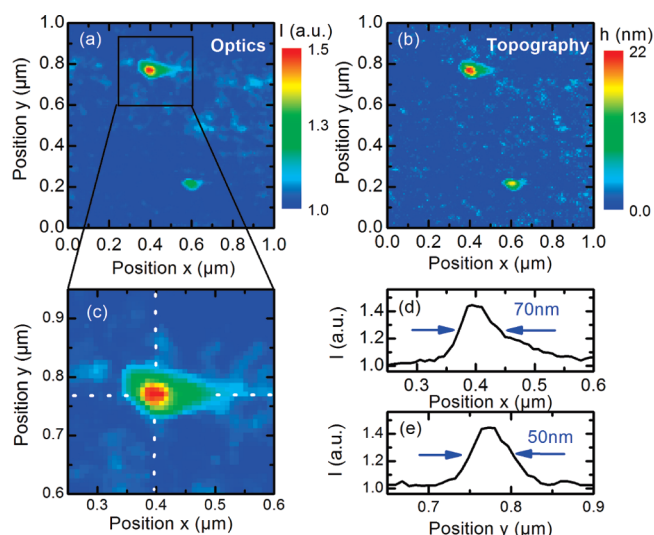


**Figure 2.** Two-dimensional optical images of individual gold nanoparticles on a glass substrate recorded by adiabatic nanofocusing optical microscopy (s-NSOM). (a) Optical s-NSOM image of two gold nanoparticles with  $<30\ \text{nm}$  radius, (b) corresponding shear-force topographical image of the nanoparticles, (c) zoomed-in image for the gold nanoparticle indicated by square in (a), and (d,e) cross sections of the optical intensity along the  $x$  and  $y$  directions (marked by dashed lines in (c)).

incidence, efficient SPP is expected for incident wavelengths close to the grating period.<sup>29</sup> Therefore, a grating period of 780 nm was chosen to allow for efficient SPP generation with a Ti:sapphire laser.

For the imaging experiments, we have prepared samples with a low density ( $1\ \mu\text{m}^{-2}$ ) of isolated spherical and elliptical gold nanoparticles with a homogeneous size distribution on a glass substrate by spin coating. Representative transmission electron microscope image of a spherical gold nanoparticle with 40 nm diameter and an elliptical gold nanoparticle with a long axis of 100 nm and a short axis of about 40 nm are shown in Figure 1c.

Figure 2a,b shows the resulting grating-coupled s-NSOM image and the corresponding topographic image obtained for small individual gold nanoparticles. In these experiments, the grating is illuminated with about 1 mW of laser light, resulting in about 50 nW of scattered light from the tip apex collected in the far field when the tip is far away from the sample. In the topographic image, the individual gold nanoparticles show a size of  $<30\ \text{nm}$  radius along the surface and a height of around 22 nm. In the grating-coupled s-NSOM image (see, e.g., Figure 2a), we observe small, extremely localized light spots with diameters of down to 30 nm at the particle position. A zoomed-in s-NSOM image for the nanoparticle indicated by the square in Figure 2a is shown in Figure 2c. Cross sections taken along the indicated dashed lines are shown in Figure 2d,e, respectively. In all figures, we find a weak, position independent background signal with an intensity level that is similar to that of light scattering from the tip apex at large tip–sample separations. In the vicinity of the nanoparticle, the normalized near-field intensity drastically increases from a value of 1.0 to more than 1.4. The cross sections show a full width at half-maximum (fwhm) of 70 nm along the  $x$ -direction and 50 nm along the  $y$ -direction, respectively. Compared to conventional scattering-type near-field images recorded with local apex excitation these profiles show at least a two-orders-of-magnitude enhancement in

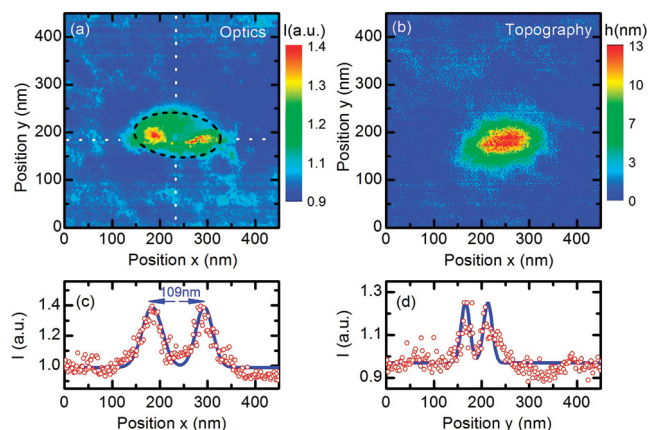


**Figure 3.** (a) Two-dimensional adiabatically focused s-NSOM image of an elliptical gold nanoparticle with  $100 \times 40 \times 15 \text{ nm}^3$  dimensions on a glass substrate. (b) Corresponding shear-force topographical image of the elliptical gold nanoparticle. (c,d) Cross sections of the optical intensity along the  $x$ - and  $y$ -directions (along the dashed lines in panel a). The strong near-field enhancement at the edges of both the long and short axis of the nanoparticle indicates that the component of the local electric field oriented along the tip axis ( $z$ -direction) is imaged.

near-field contrast, defined as the ratio of the scattering intensities from the nanoparticle and from the background.<sup>16,33,36</sup> Evidently, the chosen nonlocal optical excitation scheme greatly diminishes background-scattering from the sample surface and/or tip shaft which dominates on-apex-excitation s-NSOM images and requires the use of sophisticated modulation techniques. It is also readily apparent that the spatial image contrast in the topographic and optical images is strongly correlated. In nano-optics, such correlations are typically known as “topographic artifacts” and considered with great scepticism.<sup>37</sup>

To show that the s-NSOM images in Figure 2 do not simply reflect such topographic artifacts, we recorded light scattering images also from larger, elliptical, gold nanoparticles with  $100 \times 40 \times 15 \text{ nm}^3$  dimensions (Figure 3). The elliptical shape is clearly resolved in shear force topographic images. Now, the optical image is very different from the topographic one. We find strong, localized intensity peaks at the edges of both the long and short axis of the nanoparticle, in contrast to the regular shape of its topographical image. The two peaks along the  $x$ -axis are separated by 109 nm and have a fwhm of 40 nm, while the peaks along  $y$  are separated by 45 nm and have a fwhm of only 17 nm. The intensity maxima are again 40% higher than the position-independent background. Qualitatively, these images are readily understood. It is well-known that the near-field in the vicinity of the tip apex can to first order be approximated by that of a dipole polarization  $\vec{p}_T = \alpha \cdot E_0 \cdot \vec{e}_z$  oriented along the tip axis  $\vec{e}_z$ <sup>4,36</sup> and situated at  $\vec{r}_T$  in the center of the circularly shaped tip apex. Here,  $E_0$  denotes the incident field induced by grating coupling and  $\alpha = 8\pi\epsilon_0 r_0^3 f_e$  is the  $z$ -component of the polarizability tensor of the tip. The tip radius is denoted as  $r_0$  and  $f_e$  is a local field enhancement factor, typically being on the order of 10–20 for the tips used in our experiments.<sup>38</sup> In the quasistatic regime and treating the tip–sample coupling in the simplest possible approximation, the tip-induced near-field at position  $\vec{r}$  is  $E_T(\vec{r}) = [(3(\vec{p}_T \cdot \vec{n}) \cdot \vec{n} - \vec{p}_T) / (4\pi\epsilon_0 |\vec{r} - \vec{r}_T|^3)]$  with  $\vec{n} = (\vec{r} - \vec{r}_T) / |\vec{r} - \vec{r}_T|$ . This field now induces a dipolar polarization  $\vec{p}_S = \int \vec{\alpha}_S(\vec{r} - \vec{r}_S) \cdot E_T(\vec{r}) d\vec{r}$  in the nanoparticle, positioned at  $\vec{r}_S$  and characterized by a local

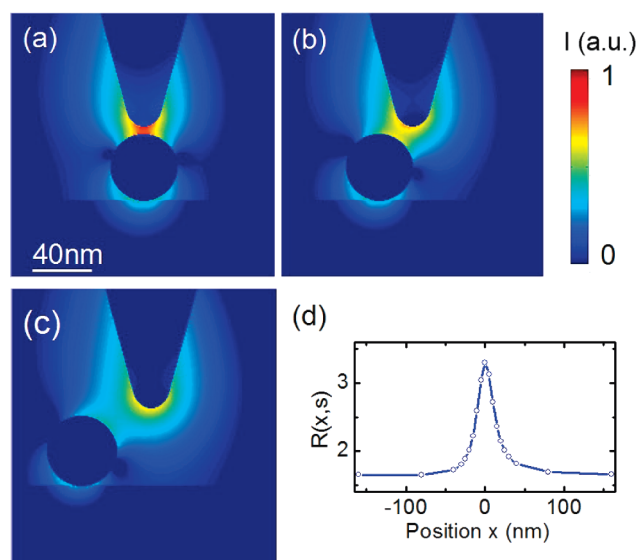
polarizability tensor  $\vec{\alpha}_S(\vec{r} - \vec{r}_S)$ . The nanoparticle polarization  $\vec{p}_S$  then acts as a source of far-field radiation  $E_S^{\text{FF}}$  that adds to the electric field  $E_T^{\text{FF}}$  scattered by the tip into the far-field. On the detector, both fields will interfere and induce a signal intensity  $I_d \propto |\vec{E}_T^{\text{FF}} + \vec{E}_S^{\text{FF}}|^2 = |\vec{E}_T^{\text{FF}}|^2 + |\vec{E}_S^{\text{FF}}|^2 + 2 \text{Re}(\vec{E}_T^{\text{FF}} \cdot \vec{E}_S^{\text{FF}})$ . This signal depends on the relative positioning of tip and sample mainly through the dependence of  $\vec{p}_S$  on  $\vec{r}_T$  and  $\vec{r}_S$ . For the case of a small, spherical nanoparticle, the isotropic polarizability tensor is a smooth and homogeneous function inside the nanoparticle. The image contrast in Figure 2 then simply reflects the spatial convolution between the near-field acting on the nanoparticle and the geometric extent of the nanoparticle polarizability. For a nanorod, however,  $\vec{\alpha}_S(\vec{r} - \vec{r}_S)$ , specifically its  $zz$ -component,  $\alpha_{S,zz}$  shows large local enhancement at the rod ends.<sup>10,39,40</sup> One therefore expects near-field images  $I_d(\vec{r}_S, \vec{r}_T)$  with peaks near the rod ends, as indeed seen in Figure 3. Retardation effects and multiple scattering events between tip and nanoparticle fields,<sup>41,42</sup> neglected above for simplicity, are believed to alter the image contrast qualitatively but not significantly.

Even though such a phenomenological model for the tip–sample coupling may account for the image shape, different pressing questions remain. The most important one certainly concerns the origin of the background signal seen in Figures 2 and 3 when the tip is positioned far away from the nanoparticles. Is this due to the field  $E_T^{\text{FF}}$  scattered by the tip apex or coming from leakage radiation from the tip shaft? Do the experimental results really confirm virtually background-free near-field imaging? Also, it is so far unknown whether the phenomenological model outlined above can indeed account for the image formation in adiabatic nanofocusing s-NSOM.

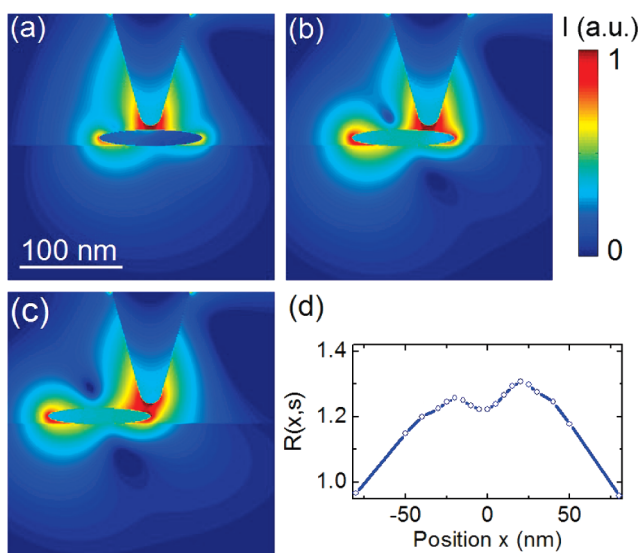
To address these issues, we have performed full three-dimensional finite-difference time domain (FDTD) simulations of such a grating-coupled adiabatically focused near-field optical microscope. In the calculations, the scattering tip is represented by a conical gold taper with an opening angle of  $30^\circ$  and a tip apex radius of 10 nm. As in the experiment, the incident light pulse, centered at  $\lambda = 780 \text{ nm}$ , is focused onto a nanoslit grating on the taper shaft, positioned at least  $4 \mu\text{m}$  away from the tip apex (see Table of Content graphics). A Drude model was used for the dielectric function of gold and the minimum grid size was 0.625 nm, ensuring numerical convergence of the field simulations.

Figure 4 shows calculations of the local electric field intensity in the vicinity of the apex of such an indirectly excited tip as it is scanned across a spherical gold nanoparticle with 20 nm radius. Two-dimensional cross sections are shown in the  $y = 0$  plane through the particle and tip centers for three different relative positions  $\vec{r}_T - \vec{r}_S$ . The tip is held at a vertical distance of 5 nm from the particle and the lateral distance is varied from 0 (a), over 20 (b), to 40 nm (c). When the tip is positioned on top of the nanoparticle, a strong dipolar nanoparticle polarization  $\vec{p}_S$ , oriented along the  $z$ -axis, is induced. Also strong field enhancement in the tip-particle gap is readily apparent. As the tip is moved away from the particle, the magnitude of the induced polarization  $\vec{p}_S$  decreases and its orientation, pointing along  $\vec{r}_T - \vec{r}_S$ , changes. With increasing distance  $\vec{r}_T - \vec{r}_S$ , tip–sample coupling rapidly decreases until, for  $\vec{r}_T - \vec{r}_S > 80 \text{ nm}$ , the field distribution is indistinguishable from that of the tip dipole alone (not shown). To mimic the experimental configuration, we approximate the intensity  $I_d$  seen with a far-field detector by  $R(x, s) = \sum_i |(E_T + E_S)(y_i, x_{\text{max}}, x_i, s)|^2$ , that is, by summing over all field intensities in a plane at  $x_{\text{max}} = 4 \mu\text{m}$ . The different  $y$ -coordinates in the detector plane are denoted as  $y_i$ . The quantities





**Figure 4.** FDTD simulation of the electric field intensity distribution at 780 nm around a gold tip, indirectly excited by grating coupling, which is raster-scanned over a spherical Au nanoparticle at 5 nm distance from the particle surface (a) when the tip is above the nanoparticle, (b) in 20 nm, and (c) in 40 nm distance from the particle center. (d) Total intensity of the near field light scattered into the far field as a function of the tip position while scanning over the nanoparticle. The tip has an apex radius of 10 nm and the 20 nm radius nanoparticle is located over a glass substrate.



**Figure 5.** FDTD simulation of the electric field intensity distribution in the near-field of a gold tip, indirectly excited by grating coupling at 780 nm and scanned over a gold nanorod at a height of 5 nm above the rod surface (a) when the tip is over the center of the nanorod, (b) in 25 nm, and (c) in 50 nm distance away from the nanorod center. (d) Total intensity of the near field light scattered into the far field as a function of the tip position while scanning over the nanoparticle. The tip has an apex radius of 10 nm and the  $100 \times 40 \times 15$  nm<sup>3</sup> elliptical nanorod is located over a glass substrate.

$x$  and  $s$  define the lateral and vertical tip–sample separations, respectively. Similarly to what is found in the experiment,  $R(x,s)$

is constant for  $x > 50$  nm and increases noticeably (by a factor of 2.0) as the tip approaches the particle. Also, the spatial extent of the locally enhanced near-field signal (30 nm fwhm) is similar to that seen in Figure 2.

When replacing the spherical nanoparticle with an elliptical nanorod one (Figure 5), strong field enhancement is seen at the edges of the nanorod and the tip–sample coupling is strongest when positioning the tip at the rod extremities. In good agreement with our experimental observations (Figure 3c),  $R(x,s)$  increases by about 30% when the tip approaches the nanorod and shows local intensity maxima at the rim of the nanorod. Even though, quite obviously, the absolute values of the local enhancement in  $R(x,s)$  depend sensitively on the exact geometric and dielectric parameters chosen for tip and particle, we find not only the qualitative but also the quantitative agreement between experiment and simulation rather remarkable. Clearly both the spatial contrast and the magnitude of the nanoparticle-induced enhanced scattering seen in Figures 2 and 3 are well reproduced in the numerical simulations. In our opinion this provides strong evidence that the “background” signal in Figures 2 and 3 is indeed given by the fundamentally limited, and unavoidable, light scattering from the tip apex. Background-free near-field imaging is achieved in the sense that the total signal recorded in the far field is solely governed by the interference between the tip-scattered fields and the induced nanoparticle field. Adiabatic nanofocusing s-NSOM hence alleviates the need for sophisticated tip–sample distance modulation schemes when attempting to extract “true” near-field contrast. Certainly, the shapes of the nanoparticles chosen in experiment and theory are not fully identical and hence details of the experimental data such as the two-maxima structure along the short axis of the particle seen in Figure 3a are not reproduced. Even better match between experiment and theory is expected for optimized nanoparticle geometries.

In summary, we have demonstrated virtually background-free imaging of electromagnetic fields in the vicinity of single metallic nanoparticles using a nonlocal grating-coupled scattering-type optical microscope. Strong near-field contrast is reached without resorting to commonly employed distance modulation techniques. The very efficient adiabatic focusing of far-field light toward a nanometer-sized spot at the tip apex shown experimentally and theoretically makes this microscope particularly attractive for linear light scattering and fluorescence imaging of densely packed nanoparticle samples. When being combined with ultrafast light pulses, the microscope might be an interesting new tool for time-resolved imaging of optical fields near surfaces or for nonlinear tip-enhanced spectroscopy.

## AUTHOR INFORMATION

### Corresponding Author

\*E-mail: christoph.lienau@uni-oldenburg.de.

## ACKNOWLEDGMENT

The authors gratefully acknowledge financial support by the Korea Foundation for International Cooperation of Science and Technology (Global Research Laboratory Project K2081500003). The work in Germany was supported by the DFG within the SPP 1391 and by personal funding for E.S. within the “EWE-Nachwuchsgruppe” (EWE AG, Oldenburg).

## REFERENCES

- (1) Inouye, Y.; Kawata, S. *Opt. Lett.* **1994**, *19* (3), 159–161.
- (2) Zenhausern, F.; Martin, Y.; Wickramasinghe, H. K. *Science* **1995**, *269* (5227), 1083–1085.
- (3) Hillenbrand, R.; Taubner, T.; Keilmann, F. *Nature* **2002**, *418* (6894), 159–162.
- (4) Bouhelier, A.; Beversluis, M.; Hartschuh, A.; Novotny, L. *Phys. Rev. Lett.* **2003**, *90*, 1.
- (5) Ichimura, T.; Fujii, S.; Verma, P.; Yano, T.; Inouye, Y.; Kawata, S. *Phys. Rev. Lett.* **2009**, *102*, 18.
- (6) Verma, P.; Ichimura, T.; Yano, T.; Saito, Y.; Kawata, S. *Laser Photon. Rev.* **2010**, *4* (4), 548–561.
- (7) Zhang, D.; Heinemeyer, U.; Stanciu, C.; Sackrow, M.; Braun, K.; Hennemann, L. E.; Wang, X.; Scholz, R.; Schreiber, F.; Meixner, A. J. *Phys. Rev. Lett.* **2010**, *104*, 5.
- (8) Esteban, R.; Vogelgesang, R.; Dorfmueller, J.; Dmitriev, A.; Rockstuhl, C.; Etrich, C.; Kern, K. *Nano Lett.* **2008**, *8* (10), 3155–3159.
- (9) Amarie, S.; Ganz, T.; Keilmann, F. *Opt. Express* **2009**, *17* (24), 21794–21801.
- (10) Schnell, M.; Garcia-Etxarri, A.; Alkorta, J.; Aizpurua, J.; Hillenbrand, R. *Nano Lett.* **2010**, *10* (9), 3524–3528.
- (11) Huber, A. J.; Keilmann, F.; Wittborn, J.; Aizpurua, J.; Hillenbrand, R. *Nano Lett.* **2008**, *8* (11), 3766–3770.
- (12) von Ribbeck, H. G.; Brehm, M.; van der Weide, D. W.; Winnerl, S.; Drachenko, O.; Helm, M.; Keilmann, F. *Opt. Express* **2008**, *16* (5), 3430–3438.
- (13) Pohl, D. W.; Denk, W.; Lanz, M. *Appl. Phys. Lett.* **1984**, *44* (7), 651–653.
- (14) Betzig, E.; Trautman, J. K. *Science* **1992**, *257* (5067), 189–195.
- (15) Michaelis, J.; Hettich, C.; Mlynek, J.; Sandoghdar, V. *Nature* **2000**, *405* (6784), 325–328.
- (16) Hillenbrand, R.; Keilmann, F. *Phys. Rev. Lett.* **2000**, *85* (14), 3029–3032.
- (17) Gomez, L.; Bachelot, R.; Bouhelier, A.; Wiederrecht, G. P.; Chang, S. H.; Gray, S. K.; Hua, F.; Jeon, S.; Rogers, J. A.; Castro, M. E.; Blaize, S.; Stefanon, I.; Lerondel, G.; Royer, P. *J. Opt. Soc. Am. B* **2006**, *23* (5), 823–833.
- (18) Chuang, C. H.; Lo, Y. L. *Opt. Express* **2008**, *16* (22), 17982–18003.
- (19) Babadjanyan, A. J.; Margaryan, N. L.; Nerkararyan, K. V. *J. Appl. Phys.* **2000**, *87* (8), 3785–3788.
- (20) Stockman, M. I. *Phys. Rev. Lett.* **2004**, *93*, No. 137404.
- (21) Issa, N. A.; Guckenberger, R. *Plasmonics* **2007**, *2* (1), 31–37.
- (22) Gramotnev, D. K.; Vogel, M. W.; Stockman, M. I. *J. Appl. Phys.* **2008**, *104*, No. 034311.
- (23) Baida, F. I.; Belkhir, A. *Plasmonics* **2009**, *4* (1), 51–59.
- (24) Nerkararyan, K. V. *Phys. Lett. A* **1997**, *237* (1–2), 103–105.
- (25) Kurihara, K.; Yamamoto, K.; Takahara, J.; Otomo, A. *J. Phys. A-Math. Theor* **2008**, *41*, No. 295401.
- (26) Durach, M.; Rusina, A.; Stockman, M. I. *Nano Lett.* **2007**, *7* (10), 3145–3149.
- (27) Verhagen, E.; Kuipers, L.; Polman, A. *Nano Lett.* **2007**, *7* (2), 334–337.
- (28) Verhagen, E.; Spasenovic, M.; Polman, A.; Kuipers, L. *Phys. Rev. Lett.* **2009**, *102*, No. 203904.
- (29) Ropers, C.; Neacsu, C. C.; Elsaesser, T.; Albrecht, M.; Raschke, M. B.; Lienau, C. *Nano Lett.* **2007**, *7*, 2784–2788.
- (30) Ropers, C.; Neacsu, C. C.; Raschke, M. B.; Albrecht, M.; Lienau, C.; Elsaesser, T. *Jpn. J. Appl. Phys.* **2008**, *47* (7), 6051–6054.
- (31) De Angelis, F.; Das, G.; Candeloro, P.; Patrini, M.; Galli, M.; Bek, A.; Lazzarino, M.; Maksymov, I.; Liberale, C.; Andreani, L. C.; Di Fabrizio, E. *Nat. Nanotechnol.* **2010**, *5* (1), 67–72.
- (32) Berweger, S.; Atkin, J. M.; Olmon, R. L.; Raschke, M. B. *J. Phys. Chem. Lett.* **2010**, 3427–3432.
- (33) Neacsu, C. C.; Berweger, S.; Olmon, R. L.; Saraf, L. V.; Ropers, C.; Raschke, M. B. *Nano Lett.* **2010**, *10* (2), 592–596.
- (34) Kim, D. S.; Hohng, S. C.; Malyarchuk, V.; Yoon, Y. C.; Ahn, Y. H.; Yee, K. J.; Park, J. W.; Kim, J.; Park, Q. H.; Lienau, C. *Phys. Rev. Lett.* **2003**, *91*, No. 143901.
- (35) Johnson, P. B.; Christy, R. W. *Phys. Rev. B* **1972**, *6* (12), 4370–4379.
- (36) Raschke, M. B.; Lienau, C. *Appl. Phys. Lett.* **2003**, *83* (24), 5089–5091.
- (37) Hecht, B.; Bielefeldt, H.; Inouye, Y.; Pohl, D. W.; Novotny, L. *J. Appl. Phys.* **1997**, *81* (6), 2492–2498.
- (38) Ropers, C.; Solli, D. R.; Schulz, C. P.; Lienau, C.; Elsaesser, T. *Phys. Rev. Lett.* **2007**, *98*, No. 043907.
- (39) Dorfmueller, J.; Vogelgesang, R.; Khunsin, W.; Rockstuhl, C.; Etrich, C.; Kern, K. *Nano Lett.* **2010**, *10* (9), 3596–3603.
- (40) Jones, A. C.; Olmon, R. L.; Skrabalak, S. E.; Wiley, B. J.; Xia, Y. N. N.; Raschke, M. B. *Nano Lett.* **2009**, *9* (7), 2553–2558.
- (41) Sun, J.; Carney, P. S.; Schotland, J. C. *J. Appl. Phys.* **2007**, *102*, No. 103103.
- (42) Deutsch, B.; Hillenbrand, R.; Novotny, L. *Nano Lett.* **2010**, *10* (2), 652–656.